Boundary Element Studies on Insulator Shape and Electric Field around HV Insulators with or without Pollution

S. Chakravorti
Electrical Engineering Department
Jadavpur University, Calcutta, India

H. Steinbigler
Institute of HV Engineering & Electric Power Transmission
Technical University Munich, Munich, Germany

ABSTRACT

Capacitive-resistive field computations are carried out around post-type HV insulators of varying shapes. The boundary element method (BEM) has been employed for electric field computations. Different insulator shapes have been obtained by varying several parameters, which define the shape of the HV insulator contour. For each insulator shape, the maximum stress occurring on the insulator surface has been determined with no surface pollution, uniform surface pollution and also partial surface pollution. For partial pollution, several cases have been studied, in which different sections of the insulator surface are polluted. Furthermore, the effect of electrode radius on the maximum stress on insulator surface has been investigated. The results obtained are presented in this paper in detail.

1 INTRODUCTION

IMPROVEMENT of HV insulating system reliability demands progress in the design criteria of insulators. Failures of outdoor HV insulators most often involve the solid-air interface of insulators. As a result, a knowledge of the field distribution around HV insulators is very important to determine the electric stresses occurring on the insulator surface, particularly on the air side of the interface.

Several researchers have computed the field distribution around HV insulators under pollution free condition. Mukherjee and Roy [1] calculated the field distribution around a disc insulator of simple geometry, Khan and Alexander [2] accurately modeled a practical disc insulator geometry and Kaana-Nkusi *et al.* [3] studied the field distribution around a section of a practical post-type insulator. Haznadar *et al.* [4] and Iravani *et al.* [5] calculated the field around a string of disc insulators. All these works have been carried out using the charge simulation method [6].

In outdoor applications, HV insulator surfaces are exposed to atmospheric as well as industrial pollution. Hence, the surface of outdoor insulators may get either uniformly polluted or partially polluted. The field around an insulator with no surface pollution is quite different from that with uniform or partial surface pollution. Therefore, it is essential to know the changes in the field distribution around an outdoor insulator caused by surface pollution of different nature and severity.

Considering uniform surface pollution, Abdel-Salam and Stanek [7] computed the field distribution around an insulator having simple geometry, and Singer [8] computed the same around a porcelain support insulator. Takuma *et al.* [9] computed the field, including either volume resistance or surface resistance, around an axi-symmetric spacer, while Kumar and Nagabhushana [10] computed the same around an impulse generator wave-tail resistor. Chakravorti and Mukherjee [11] computed the field around a post type insulator with uniform or non-uniform surface pollution. However, all these studies have been carried out using the charge simulation method. Tang and Raghuveer [12] calculated the field around a HVDC wall bushing with nonuniform surface pollution using the finite element method (FEM).

It has been observed by researchers that the analysis of axi-symmetric electric field distribution by integral methods such as the charge simulation method (CSM) or boundary element method (BEM) is more convenient than by differential techniques such as FEM. It has further been noted that a major problem in CSM is the uncomfortable and subjective placement of simulation charges, which can be obviated by the use of BEM. In recent years the BEM has been successfully employed for electric field calculation in complex 2-D and 3-D systems [13–15] and field calculations including volume and surface resistivities by BEM have also been reported [16–20]. Because the field distribution around an insulator is axi-symmetric in nature and depends upon the insulator geometry, the influence of insulator shape on the field distri-

1070-9878/0/ $3.00 © 2000 IEEE

bution around a post-type insulator has been studied by BEM. Several parameters, which define the shape of insulator contour, are varied and their effects on the stresses occurring on the insulator surface are studied, in the presence as well as in the absence of surface pollution. In the case of partial surface pollution, the effects of the zone which is polluted also are determined. In addition, for a given insulator shape, the effects of electrode radius on electric stresses with or without surface pollution have been studied. The results of all these studies are presented in detail in this paper.

2 INSULATOR CONFIGURATIONS

Two types of post-insulator configurations, as shown in Figures 1(a) and (b) respectively, are considered for capacitive-resistive field calculations. In both cases, the following are taken into consideration

1. the insulator is made of porcelain and is surrounded by air,
2. the insulator is stressed between a pair of electrodes, as shown in Figures 1(a) and (b),
3. the bottom electrode is taken as grounded, while the voltage applied to the live electrode is of unity magnitude,
4. the applied voltage is sinusoidal, with frequency of 50 Hz.

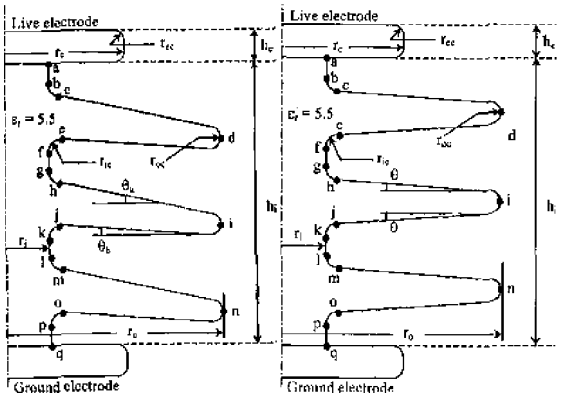

Figure 1. (a) Axi-symmetric post-type insulator configuration 1. (b) Axi-symmetric post-type insulator configuration 2.

Therefore, the insulator-electrode arrangements under consideration have axi-symmetric configuration with two dielectrics. The two configurations shown in Figures 1(a) and (b) differ in the shape of the insulator sheds. For configuration 1 as shown in Figure 1(a), upper as well as lower insulator surfaces have negative slopes, and the slope angle for the upper surface θ_a is always higher than that for the lower surface θ_b. In the case of configuration 2, as shown in Figure 1(b), the upper insulator surface has a negative slope and the lower surface a positive one. However, the slope angle θ for both these surfaces are taken to be equal.

3 METHOD OF SIMULATION

The technique described below for the calculation of axi-symmetric capacitive-resistive field distribution is based on the BEM [21]. In this method the electrode and dielectric boundaries are discretized into several boundary elements and a suitable distribution function is introduced for the equivalent surface charges along the discrete boundary elements. Then the electric field in the region of interest is considered to be caused by the equivalent surface charges along the boundary elements. The equivalent surface charges are determined by solving a system of integral equations, which are obtained by satisfying the following boundary conditions

1. On the conductor surfaces with known potential, the prescribed values of the potential function are maintained,
2. On the dielectric-dielectric boundaries, the condition for the normal component of the electric flux density D_n is maintained.

For any point I on the electrode surface, the potential in the capacitive-resistive field distribution is calculated according to the relationship

$$\overline{\phi}(I) = \frac{1}{4\pi\varepsilon_o}\left[\sum_{p=1}^{P}\int_{S_p}\frac{\overline{\sigma}(M)}{r_{\mathrm{MI}}}\,dS_p + \sum_{d=1}^{D}\int_{S_d}\frac{\overline{\sigma}(N)}{r_{\mathrm{NI}}}\,dS_d\right] \quad (1)$$

where $I \in S_p$, and $p = 1, 2 \ldots, P$, σ is the equivalent surface charge density at any node, S_p the conductor boundary, $p = 1, 2, \ldots P$, S_d the dielectric-dielectric boundary, $d = 1, 2, \ldots, D$, M the index of the boundary nodes lying on the conductor surface, N the index of the boundary nodes lying on the dielectric-dielectric interface.

In Equation (1), the potential and charge densities are taken as complex quantities instead of having real values, only for calculating the capacitive-resistive field. The complex quantities are marked by an overbar (as in $\overline{\sigma}$) in this paper.

If $\overline{\sigma_s}$ is the bound surface charge density on the dielectric-dielectric boundary, then the boundary condition at any point i on the interface of two dielectrics can be written as

$$\varepsilon_1\overline{E_{1n}}(i) - \varepsilon_2\overline{E_{2n}}(i) = \overline{\sigma_s}(i) \quad (2)$$

where ε_x is the permittivity of dielectric x, $x = 1, 2$ and $\overline{E_{xn}}$ is the normal component of the electric field intensity at the dielectric x side of interface, $x = 1, 2$. $\overline{E_{1n}}$ and $\overline{E_{2n}}$ at the point i can be calculated with orientation towards the dielectric 1 side, as in [21].

$$\begin{aligned}\overline{E_{1n}}(i) &= \overline{E_n}(i) + \frac{\overline{\sigma}(i)}{2\varepsilon_o}\\ \overline{E_{2n}}(i) &= \overline{E_n}(i) - \frac{\overline{\sigma}(i)}{2\varepsilon_o}\end{aligned} \quad (3)$$

where $\overline{E_n}(i)$ is the normal component of the electric field intensity at the node i by charge densities at all the nodes [14, 15].

For fields including volume and surface resistivities, $\overline{\sigma_s}(i)$ is to be determined from the general condition of the current density vector at the point i [22]. Considering isotropic materials and sinusoidal fields, this condition can be written as follows [16]

$$\frac{\overline{E_{1n}}(i)}{\rho_{v1}} - \frac{\overline{E_{2n}}(i)}{\rho_{v2}} + \Delta\overline{J_s}(i) + \mathrm{i}\omega\overline{\sigma_s}(i) = 0 \quad (4)$$

where ρ_{vx} is the volume resistivity of dielectric x, $x = 1, 2$ and

$$\begin{aligned}\Delta\overline{J_s}(i) = \frac{1}{S(i)}\Bigg[&\overline{\phi}(i)\left\{\frac{1}{R(i)} + \frac{1}{R(i+1)}\right\}\\ &-\frac{\overline{\phi}(i+1)}{R(i+1)} - \frac{\overline{\phi}(i-1)}{R(i)}\Bigg]\end{aligned} \quad (5)$$

Equations (2) to (5) can be combined together in the following form

$$\frac{2(\overline{\varepsilon_1}-\overline{\varepsilon_2})}{(\overline{\varepsilon_1}+\overline{\varepsilon_2})}\overline{E}_n(i)-\frac{2\mathrm{i}}{\omega S(i)(\overline{\varepsilon_1}+\overline{\varepsilon_2})}\times$$
$$\left[\overline{\phi}(i)\left\{\frac{1}{R(i)}+\frac{1}{R(i+1)}\right\}-\frac{\overline{\phi}(i+1)}{R(i+1)}-\frac{\overline{\phi}(i-1)}{R(i)}\right]+\frac{\overline{\sigma}(i)}{\varepsilon_o}=0 \quad (6)$$

where

$$\overline{\varepsilon}_x=\varepsilon_o\varepsilon_{rx}-\frac{\mathrm{i}}{\omega\rho_{vx}} \quad (7)$$

and where $x = 1, 2$, $\omega = 2\pi f$, f is the frequency, $S(i)$ is a small area, $R(i)$ and $R(i+1)$ are surface resistances around the node i, respectively. The methods of calculation of $S(i)$, $R(i)$ and $R(i+1)$ are described in [11]. The nodes with the indices $i-1$, i and $i+1$ are three consecutive nodes on the dielectric-dielectric boundary. The ordering of the nodes for the use of indices $i-1$, i and $i+1$ has been discussed in [9].

For the calculation of axi-symmetric fields, straight line and elliptic arc elements are used. A linear basis function is assumed for the description of charge distribution along the boundary element between the nodes. For the definition of boundary nodes and elements, adaptive discretization in conformity with electric stress variation has been implemented in this work and the same discretization criterion has been used in all investigations presented in this paper.

For capacitive-resistive field calculation, uniform surface pollution is simulated by a uniform resistivity ρ_s along the insulator contour. Non-uniform pollution of the insulator surface is simulated by considering different values of ρ_s at different locations on the insulator surface. No volume conduction has been considered in this purpose and, hence, volume resistivities for both porcelain and air have been taken to be infinite.

A comprehensive program named TWIN based on the formulations described above has been developed and the investigation results described here have been obtained using this program.

4 RESULTS AND DISCUSSION

For an insulator with surface pollution, the field distribution may be capacitive, capacitive-resistive or resistive, depending upon the severity of surface pollution, while for a pollution-free insulator the field is capacitive in nature. The severity of surface pollution has been represented quantitatively by earlier researchers [9, 11, 20] by the range of ρ_s within which changes in the nature of field distribution take place. Hence, considering uniform surface pollution, field computations are at first carried out to determine the range of ρ_s, within which the field distribution changes from capacitive to resistive in nature. It has been observed here that the field is capacitive for $\rho_s \geqslant 10^{11}\Omega$ and is resistive for $\rho_s \leqslant 10^7\Omega$. For the intermediate values of ρ_s, the field is capacitive-resistive.

Field computations are carried out for different shapes of the two types of insulator contours described in Figures 1(a) and (b). These different shapes are obtained by varying several parameters, which define the shape of insulator contour. The parameters studied in this work are the slope angle of the insulator shed θ_u, θ_b and θ, the insulator shed radius r_o, the insulator core radius r_i, the axial height h_i, the insulator shed outer corner radius r_{oc}, and the inner corner radius r_{ic}. To investigate the influences of various parameters on the electric field distribution, the values of the parameters under consideration are varied within the range of practical applications. It may be noted here that the number of insulator sheds is taken to be 3 in all cases under consideration from the point of view of actual usage. However, neither the formulations presented nor the program mentioned earlier is limited to a given number of sheds only, but are of generalized nature. For each of these insulator shapes, electric stresses are calculated along the insulator surface for three different cases as follows

1. no surface pollution, *i.e.* capacitive field, with $\rho_s = 10^{11}\ \Omega$,
2. uniform surface pollution with $\rho_s = 10^7\ \Omega$,
3. partial surface pollution for which ρ_s is set at $10^7\ \Omega$ along the section a-d of the insulator surface, *i.e.* from the point of contact of the insulator with the live electrode, to the tip of the topmost insulator shed, while $\rho_s = \infty$ along the rest of the insulator surface.

The highest stresses occurring on the insulator surface are denoted by E_{mnp} for no surface pollution, E_{mup} for uniform surface pollution and E_{mpp} for partial surface pollution and are presented in this paper for different insulator shapes. The electric stresses are calculated on the air-side of the porcelain-air interface and are presented in a normalized format (V/m)/V, *i.e.* as electric field intensity per unit magnitude of applied potential difference. For each insulator contour considered, the creepage length L_{cr} has been calculated also, and is presented here in m. The results obtained are discussed in detail in the following Sections.

4.1 EFFECT OF THE SLOPE ANGLE

For field computations in this case, the following parameters have been kept constant: $r_o = 0.08$ m, $r_i = 0.025$ m, $h_i = 0.15$ m, $r_{oc} = 0.002$ m and $r_{ic} = 0.0045$ m. The electrode dimensions also are kept constant as follows: electrode radius $r_e = 0.035$ m, electrode corner radius $r_{ec} = 0.005$ m and electrode height $h_e = 0.05$ m.

For configuration 1 as shown in Figure 1(a), results have been obtained for different values of θ_u and θ_b. The values of θ_b considered are 0^0, 5^0 and 10^0 respectively and for each θ_b the values of θ_u are chosen such that $(\theta_u - \theta_b)$ varies from 5^0 to 20^0 in steps of 5^0. Table 1 presents the values of L_{cr}, E_{mnp}, E_{mup} and E_{mpp} for all the insulator shapes thus obtained. From Table 1 it may be noted that as θ_u increases, within the range given above, for a given θ_b, L_{cr} decreases by 5.7% to 6.8%, E_{mnp} increases by 18.7% to 19.0%, E_{mup} decreases by 4.2% to 4.6% and E_{mpp} decreases by 2.2% to 4.3%. On the other hand, when θ_b increases from 0^0 to 10^0 for a given value of θ_u, *e.g.* 20^0, L_{cr} increases by 9.7%, E_{mnp} decreases significantly by 14.1%, E_{mup} increases by 3.6% and E_{mpp} decreases by 7.2%.

The computed values thus indicate that a higher θ_u for a given θ_b does not yield notable reduction in stresses, but does lower L_{cr}. On the other hand, a higher θ_b for a given θ_u, with the condition that $\theta_u > \theta_b$, does give improved stresses and higher L_{cr}.

For configuration 2 as shown in Figure 1(b), the values used for θ vary from 3^0 to 15^0 in steps of 3^0 and the results of computations are presented in Table- 2. In this case it may be noted that as θ increases, L_{cr} decreases by 11.6%, E_{mnp} increases strongly by 36.9%, E_{mup} and E_{mpp} decrease by 5.7% and 3.7% respectively. Analysis of the results thus shows that an increase in θ for configuration 2 does not provide notable improvement in electric stresses, but does reduce L_{cr}.

Table 1. Effect of the slope angle of insulator shed on the creepage length and maximum stress on the insulator surface for configuration 1 of Figure 1(a). L_{cr} Creepage length of insulator in meters. E_{mnp} Highest stress without surface pollution. E_{mup} Highest stress with uniform surface pollution. E_{mpp} Highest stress with partial surface pollution. θ_b and θ_u are in degree (°).

Θ_b	Θ_u	L_{cr}	E_{mnp}	E_{mup}	E_{mpp}
0	5	0.3685	21.24	52.38	77.87
	10	0.3595	22.59	51.42	77.01
	15	0.3511	23.83	50.61	76.36
	20	0.3433	25.28	49.99	76.10
5	10	0.3753	21.11	52.22	74.56
	15	0.3699	22.38	51.78	73.94
	20	0.3591	23.71	50.85	73.26
	25	0.3518	25.12	50.03	72.87
10	15	0.3846	20.49	52.28	70.81
	20	0.3768	21.70	51.77	70.59
	25	0.3695	23.09	51.03	69.68
	30	0.3626	24.33	49.89	67.76

Table 2. Effect of the slope angle of insulator shed on the creepage length and maximum stress on the insulator surface for configuration 2 of Figure 1(b).

Θ	3	6	9	12	15
L_{cr}	0.3664	0.3549	0.3441	0.3336	0.3237
E_{mnp}	19.78	21.21	22.54	23.97	27.08
E_{mup}	52.20	51.36	51.14	50.34	49.22
E_{mpp}	74.93	74.47	73.99	72.87	72.13

4.2 EFFECT OF INSULATOR SHED RADIUS

The following parameters are kept constant for field computations, in this case $r_i = 0.025$ m, $h_i = 0.15$ m, $r_{oc} = 0.002$ m, $r_{ic} = 0.0045$ m, $r_c = 0.035$ m, $r_{cc} = 0.005$ m and $h_c = 0.05$ m. The values of insulator shed radius r_o are varied from 0.06 m to 0.1 m in steps of 0.01 m.

Results have been computed for several shapes of configuration 1 and configuration 2 as reported in Tables 1 and 2 respectively, but the results for only two representative shapes are presented from Table 3 onwards. These two cases are configuration 1 with $\theta_u = 20^0$ and $\theta_b = 10^0$ and configuration 2 with $\theta = 3^0$ respectively. Table 3 shows that for configuration 1, when r_o increases within the given range, L_{cr} increases by 86.2%, E_{mnp} decreases strongly by 22.8%, E_{mup} decreases by 6.5% and E_{mpp} decreases significantly by 16.2%. Again, for configuration 2 as r_o increases within the same range, L_{cr} increases by 90.2%, notably E_{mnp} increases and E_{mpp} decreases by 13.6% and 13.1% respectively, while E_{mup} decreases by a relatively smaller amount, 4.9%.

A higher value of r_o, in addition to increasing L_{cr}, does improve the results considerably for configurations 1 and 2 causing lower stresses in the presence of surface pollution, but at the same time increases the stress in the absence of surface pollution.

It may also be observed that, for a given r_o within the specified range, E_{mnp} for configuration 1 is greater than E_{mnp} for configuration 2 in the range 0.06 m $\leqslant r_o \leqslant$ 0.08 m and the difference gradually decreases from 26.9% to 1.2% as r_o increases from 0.06 m to 0.08 m. For $r_o = 0.09$ m, E_{mnp} values are almost equal for configuration 1 and 2, while for $r_o = 0.1$ m, E_{mnp} for configuration 2 is 7.7% higher than that for configuration 1. Further, for a given r_o within the specified range E_{mup} values are nearly the same for both configuration 1 and 2, the values of configuration 2 being slightly on the higher side and E_{mpp} for configuration 1 is less than that for configuration 2, the difference increasing from 4.0% to 9.7% with increasing r_o.

Table 3. Effect of the insulator shed radius on the creepage length and maximum stress on the insulator surface. θ_b, θ_u and θ are in degree (°).

r_o m		Config 1 $\Theta_u = 20, \Theta_b = 10$	Config 2 $\Theta = 3$
0.06	L_{cr}	0.2633	0.2524
	E_{mnp}	25.24	18.45
	E_{mup}	53.21	53.15
	E_{mpp}	75.55	79.90
0.07	L_{cr}	0.3201	0.3094
	E_{mnp}	22.97	19.15
	E_{mup}	52.54	52.96
	E_{mpp}	74.37	77.37
0.08	L_{cr}	0.3768	0.3663
	E_{mnp}	21.70	19.78
	E_{mup}	51.77	52.20
	E_{mpp}	70.59	74.93
0.09	L_{cr}	0.4355	0.4233
	E_{mnp}	20.49	20.25
	E_{mup}	50.76	51.56
	E_{mpp}	66.99	71.89
0.1	L_{cr}	0.4903	0.4802
	E_{mnp}	19.47	20.97
	E_{mup}	49.74	50.54
	E_{mpp}	63.29	69.42

4.3 EFFECT OF INSULATOR CORE RADIUS

In this case the constant parameters for field computations are as follows: $r_o = 0.08$ m, $h_i = 0.15$ m, $r_{oc} = 0.002$ m, $r_{ic} = 0.0045$ m, $r_c = 0.035$ m, $r_{cc} = 0.005$ m and $h_c = 0.05$ m. Insulator core radius r_i is varied from 0.015 to 0.025 m in steps of 0.002 m.

The results of computations are tabulated in Table 4. For configuration 1 as in Table 4, L_{cr} decreases by 13.1% and E_{mnp} decreases by 1.6% with the increase in r_i within the range mentioned above. On the other hand, as r_i increases within the same range, E_{mup} and E_{mpp} for configuration 1 increase by 0.15% and 4.5% respectively. For configuration 2 as in Table 4, with the increase in r_i within the same range, L_{cr} decreases by 13.4% and E_{mnp}, E_{mup} and E_{mpp} increase by 1.3%, 0.36% and 0.83% respectively.

The results discussed here show that as r_i is increased, L_{cr} decreases and the stresses are increased for configuration 1 as well as for configuration 2, leaving aside E_{mnp} for configuration 1. However, the incremental changes in the stresses are comparatively low. Again, for a given r_i within the specified range, E_{mnp} and E_{mup} for configuration 1 are greater than those for configuration 2 and E_{mpp} for configuration 1 is less than that for configuration 2. The differences vary between 8.8% to 11.5%, 0.6% to 0.8% and 6.2% to 10.1% for E_{mnp}, E_{mup} and E_{mpp} respectively.

Table 4. Effect of the insulator core radius on the creepage length and maximum stress on the insulator surface. θ_b, θ_u and θ are in degree (°).

r_i m		Config 1 $\Theta_u = 20, \Theta_b = 10$	Config 2 $\Theta = 3$
0.015	L_{cr}	0.4335	0.4233
	E_{mmp}	22.06	19.52
	E_{mup}	51.74	52.05
	E_{mpp}	67.53	74.34
0.017	L_{cr}	0.4222	0.4119
	E_{mmp}	22.03	19.53
	E_{mup}	51.77	52.13
	E_{mpp}	68.31	74.37
0.019	L_{cr}	0.4108	0.4005
	E_{mmp}	21.93	19.54
	E_{mup}	51.77	52.13
	E_{mpp}	68.54	74.73
0.021	L_{cr}	0.3995	0.3891
	E_{mmp}	21.85	19.56
	E_{mup}	51.78	52.15
	E_{mpp}	68.89	74.75
0.023	L_{cr}	0.3881	0.3777
	E_{mmp}	21.81	19.62
	E_{mup}	51.79	52.20
	E_{mpp}	69.47	74.93
0.025	L_{cr}	0.3768	0.3663
	E_{mmp}	21.70	19.78
	E_{mup}	51.82	52.24
	E_{mpp}	70.59	74.96

Table 5. Effect of the insulator axial height on the creepage length and maximum stress on the insulator surface. θ_b, θ_u and θ are in degree (°).

h_i m		Config 1 $\Theta_u = 20, \Theta_b = 10$	Config 2 $\Theta = 3$
0.12	L_{cr}	0.3468	0.3363
	E_{mmp}	22.28	22.08
	E_{mup}	54.61	55.01
	E_{mpp}	72.88	77.33
0.14	L_{cr}	0.3668	0.3563
	E_{mmp}	22.06	20.32
	E_{mup}	52.60	53.07
	E_{mpp}	71.01	75.59
0.16	L_{cr}	0.3868	0.3763
	E_{mmp}	21.33	19.14
	E_{mup}	51.10	51.52
	E_{mpp}	68.35	74.48
0.18	L_{cr}	0.4068	0.3963
	E_{mmp}	20.92	18.04
	E_{mup}	49.87	50.25
	E_{mpp}	67.53	73.29
0.20	L_{cr}	0.4268	0.4163
	E_{mmp}	20.59	17.09
	E_{mup}	48.92	49.22
	E_{mpp}	66.68	72.39

4.4 EFFECT OF INSULATOR AXIAL HEIGHT

The parameters kept constant for field computations in this case are as follows: $r_o = 0.08$ m, $r_i = 0.025$ m, $r_{oc} = 0.002$ m, $r_{ic} = 0.0045$ m, $r_e = 0.035$ m, $r_{ec} = 0.005$ m and $h_e = 0.05$ m. The values of insulator axial height h_i are varied from 0.12 to 0.2 m in steps of 0.02 m and the results are given in Table 5.

Analyses of the results show that, as h_i increases within the range given above, for configuration 1, L_{cr} increases by 23.1%, E_{mmp}, E_{mup} and E_{mpp} decrease by 7.6%, 10.4% and 8.5% respectively and for configuration 2, L_{cr} increases by 23.8%, E_{mmp}, E_{mup} and E_{mpp} decrease by 22.6%, 10.5% and 6.4% respectively.

In other words, a higher h_i increases L_{cr} and reduces the stresses for both configuration 1 and 2 in the presence as well as in the absence of surface pollution.

Further, for a given h_i within the range specified above, E_{mup} and E_{mpp} for configuration 1 are lower than those for configuration 2, the differences being in the ranges of 0.6% to 0.9% and 6.1% to 8.9% for E_{mup} and E_{mpp} respectively. But E_{mmp} for configuration 1 is greater than that for configuration 2, the difference being in the range 0.9% to 17.0%.

4.5 EFFECT OF INSULATOR SHED OUTER CORNER RADIUS

In this case the following parameters are kept constant for field computations: $r_o = 0.08$ m, $r_i = 0.025$ m, $h_i = 0.15$ m, $r_{ic} = 0.0045$ m, $r_e = 0.035$ m, $r_{ec} = 0.005$ m and $h_e = 0.05$ m. Insulator shed outer corner radius r_{oc} is varied from 0.0015 to 0.004 m in steps of 0.0005 m.

The computational results are presented in Table-6. Table 6 shows that for configuration 1, as r_{oc} increases within the range mentioned above, L_{cr} decreases by 1.5%, E_{mmp} increases by 9.6% and E_{mup} and E_{mpp} decrease by 35.6% and 30.7% respectively. Similarly in the case of configuration 2, with the increase in r_{oc} within the same range, L_{cr} decreases by 1.6%, E_{mmp} increases by 12.5% and E_{mup} and E_{mpp} decrease by 35.8% and 32.1% respectively. It is significant to note here that for both configuration 1 and 2, the maximum stresses on the insulator surface in the presence of surface pollution is greatly reduced as r_{oc} is increased. However, an increased r_{oc} also reduce L_{cr} to some extent.

Again it may also be noted that, for a given r_{oc} within the specified range, E_{mmp} for configuration 1 is greater than E_{mup} for configuration 2, the difference being in the range 6.5% to 9.5%. On the other hand, E_{mup} and E_{mpp} for configuration 1 are lower than those for configuration 2, the ranges of difference being 0.8% to 1.4% and 5.8% to 8.35% for E_{mup} and E_{mpp} respectively.

4.6 EFFECT OF INSULATOR SHED INNER CORNER RADIUS

There are two inner corners of the insulator shed to be considered, one each at the upper surface and lower surface of the insulator shed respectively. The radii of both the inner corners are taken to be equal in the present study. The value of the insulator shed inner corner radius r_{ic} is varied from 0.003 to 0.006 m in steps of 0.001 m. The other parameters, which are considered to be constant for field computations are as follows: $r_o = 0.08$ m, $r_i = 0.025$ m, $h_i = 0.15$ m, $r_{oc} = 0.002$ m, $r_e = 0.035$ m, $r_{ec} = 0.005$ m and $h_e = 0.05$ m.

The computed results are tabulated in Table-7. The results show that as r_{ic} is increased within the range given above, for configuration 1 L_{cr} decreases by 13.3%, E_{mmp} and E_{mup} decrease by 1.9% and 0.15% respectively and E_{mpp} is maximum for $r_{ic} = 0.0045$ m. But

Table 6. Effect of the insulator shed outer corner radius on the creepage length and maximum stress on the insulator surface. θ_b, θ_u and θ are in degree (°).

r_{oc} m		Config 1 $\Theta_u = 20, \Theta_b = 10$	Config 2 $\Theta = 3$
0.0015	L_{cr}	0.3779	0.3675
	E_{mnp}	21.24	19.21
	E_{mup}	58.64	59.48
	E_{mpp}	77.35	83.41
0.002	L_{cr}	0.3768	0.3663
	E_{mnp}	21.70	19.78
	E_{mup}	51.77	52.20
	E_{mpp}	70.59	74.93
0.0025	L_{cr}	0.3756	0.3652
	E_{mnp}	22.02	20.29
	E_{mup}	46.74	47.17
	E_{mpp}	63.73	68.37
0.003	L_{cr}	0.3745	0.3641
	E_{mnp}	22.24	20.79
	E_{mup}	42.98	43.37
	E_{mpp}	58.92	63.85
0.0035	L_{cr}	0.3734	0.3629
	E_{mnp}	22.80	21.23
	E_{mup}	40.04	40.43
	E_{mpp}	56.10	59.85
0.004	L_{cr}	0.3722	0.3618
	E_{mnp}	23.28	21.61
	E_{mup}	37.74	38.19
	E_{mpp}	53.55	56.65

the difference between the minimum value of E_{mpp} which occurs for $r_{ic} = 0.003$ m and this maximum value of E_{mpp}, is 2.7%. Again, for configuration 2, with the increase in r_{ic} within the same range, L_{cr} decreases by 15.5%, E_{mnp} decreases by 8.3%, E_{mup} increases by 0.25% and E_{mpp} is minimum for $r_{ic} = 0.0045$ m. The difference between this minimum value of E_{mpp} and the maximum value of E_{mpp}, which occurs for $r_{ic} = 0.006$ m is only 0.46%. It may thus be noted that r_{ic} has very little effect on the maximum stresses occurring on the insulator surface, particularly with surface pollution. But an increased r_{ic} reduces L_{cr} by a significant amount.

4.7 EFFECT OF ELECTRODE RADIUS

Apart from studying the effects of various parameters defining the shape of the insulator contour, the effects of the electrode radius on the electric stresses occurring on the insulator surface have also been studied. The value of electrode radius r_e is varied from 0.035 to 0.06 m in steps of 0.005 m. The parameters kept constant for field computations in this case are as follows: $r_o = 0.08$ m, $r_i = 0.025$ m, $h_i = 0.15$ m, $r_{oc} = 0.002$ m, $r_{ic} = 0.0045$ m, $r_{ec} = 0.005$ m and $h_e = 0.05$ m.

The results of computations for different values of r_e are presented in Table 8. Table 8 shows that, as r_e is increased within the range mentioned above, for configuration 1 E_{mnp} increases by 22.1%, E_{mup} and E_{mpp} decrease by 11.2% and 6.5% respectively and for configuration 2 E_{mup} and E_{mpp} decrease by 13.7% and 8.4% respectively. E_{mnp} for configuration 2 is minimum for $r_e = 0.05$ m and the difference between this minimum value and the maximum value of E_{mnp}, which occurs for $r_e = 0.035$ m, is 19.1%. Thus it is found that a higher value of

Table 7. Effect of the insulator shed inner corner radius on creepage length and maximum stress on the insulator surface. θ_b, θ_u and θ are in degree (°).

r_{ic} m		Config 1 $\Theta_u = 20, \Theta_b = 10$	Config 2 $\Theta = 3$
0.003	L_{cr}	0.4037	0.3971
	E_{mnp}	21.96	20.91
	E_{mup}	51.83	52.18
	E_{mpp}	68.72	75.08
0.004	L_{cr}	0.3858	0.3766
	E_{mnp}	21.93	20.01
	E_{mup}	51.81	52.19
	E_{mpp}	70.28	75.01
0.0045	L_{cr}	0.3768	0.3663
	E_{mnp}	21.70	19.78
	E_{mup}	51.77	52.20
	E_{mpp}	70.59	74.93
0.005	L_{cr}	0.3678	0.3561
	E_{mnp}	21.65	19.47
	E_{mup}	51.76	52.23
	E_{mpp}	69.24	75.22
0.006	L_{cr}	0.3498	0.3356
	E_{mnp}	21.54	19.17
	E_{mup}	51.75	52.31
	E_{mpp}	69.01	75.28

Table 8. Effect of the electrode radius on the maximum stress on the insulator surface. θ_b, θ_u and θ are in degree (°).

r_e m		Config 1 $\Theta_u = 20, \Theta_b = 10$	Config 2 $\Theta = 3$
0.035	E_{mnp}	21.70	19.78
	E_{mup}	51.77	52.20
	E_{mpp}	70.59	74.93
0.04	E_{mnp}	22.85	17.76
	E_{mup}	50.89	51.07
	E_{mpp}	70.01	74.31
0.045	E_{mnp}	23.95	16.86
	E_{mup}	49.88	49.89
	E_{mpp}	69.27	73.10
0.05	E_{mnp}	24.94	16.61
	E_{mup}	48.73	48.52
	E_{mpp}	68.37	72.04
0.055	E_{mnp}	25.80	17.46
	E_{mup}	47.44	46.91
	E_{mpp}	67.28	70.33
0.06	E_{mnp}	26.48	18.18
	E_{mup}	45.97	45.03
	E_{mpp}	65.96	68.65

r_e reduces the maximum stress on the insulator surface in the presence of surface pollution. Further, for a given r_e within the specified range, E_{mnp} for configuration 1 is higher than that for configuration 2 and E_{mpp} for configuration 1 is lower than that for configuration 2, the difference being in the range of 8.8% to 33.4% and 4.1% to 6.1% for E_{mnp} and E_{mpp} respectively. E_{mup} for configuration 1 is nearly equal to E_{mup} for configuration 2 when $r_e = 0.045$ m. Again, for a given r_e, E_{mup} for configuration 1 is less than that for configuration 2 when $r_e < 0.045$ m and is higher than that for configuration 2 when $r_e > 0.045$ m, the differences lying within 0.35% to 2.0%.

Table 9. Effect of the partial surface pollution zone on the maximum stress on the insulator surface. θ_b, θ_u and θ are in degree (°).

Partial pol. zone	E_{mpp} Conf 1	E_{mpp} Conf 2	Partial pol. zone	E_{mpp} Conf 1	E_{mpp} Conf 2
a - d	70.59	74.93	a - l	17.36	11.42
a - f	59.82	64.71	a - d g - i	63.74	75.37
a - g	62.98	71.65	a - d f - i	58.79	80.49
a - i	76.80	66.93	a - d g - i i - n	64.22	76.52
a - k	60.22	57.95	a - d f - i k - n	71.23	90.53

4.8 EFFECT OF THE ZONE OF PARTIAL SURFACE POLLUTION

In the earlier Sections of this paper, the zone of partial surface pollution is considered to be the section a-d of the insulator surface, Figure 1. In addition to this zone, studies have been carried out also for several other zones of partial surface pollution. These studies include cases, where multiple sections of the insulator surface, which need not be continuous, are considered to be polluted simultaneously. In each case ρ_s in the polluted zone is taken to be $10^7\Omega$ and that be infinite in the other parts of the insulator surface. Table 9 presents the results of these computations. In all these field computations the following parameters are taken to be constant: $r_o = 0.08$ m, $r_i = 0.025$ m, $h_i = 0.15$ m, $r_{oc} = 0.002$ m, $r_{ic} = 0.0045$ m, $r_c = 0.035$ m, $r_{ec} = 0.005$ m and $h_e = 0.05$ m.

In Table 9, results for six different cases of partially polluted insulator surface where the polluted sections are taken to be continuous, are given. For both configuration 1 and 2, E_{mpp} is highest in the case, when the section a-l of Figure 1 of the insulator surface is polluted. Compared to the values of E_{mpp} in the case when the section a-d of Figure 1 is polluted, which are discussed in the earlier Sections, these highest values of E_{mpp} are 66.2% and 48.7% higher for configuration 1 and 2 respectively. Results for four different cases of discontinuous multiple insulator sections, which are polluted simultaneously are also reported in Table 9. Compared to the case when the section a-d of Figure 1 is polluted, E_{mpp} for multiple polluted zones for configuration 1 are lower or nearly equal and the same for configuration 2 are higher. In other words, for simultaneous multiple polluted zones on the insulator surface, E_{mpp} for configuration 1 is lower than that for configuration 2. For multiple polluted zones, worst results are obtained when the sections a-d, f-i and k-n of Figure 1 are polluted simultaneously. However, the stresses for this case are much lower, compared to the case when the section a-l of Figure 1 is polluted only.

5 CONCLUSIONS

EFFECTS of various parameters, which define the shape of insulator contour, on the electric stresses occurring on the insulator surface with or without surface pollution have been studied by BEM. Considering the maximum stress on insulator surface it has been found that better results may be obtained in the case of configuration 1 and 2 for (1) a higher r_o, particularly in the presence of surface pollution, and (2) higher h_i and r_{oc}, both with or without surface pollution.

Similarly in the case of configuration 1, better results may be obtained for a higher θ_b for a given θ_u with the condition $\theta_u > \theta_b$. It has also been noted that r_i and r_{ic} have negligible effects on the maximum stresses. Studies also show that the zone of partial surface pollution influence the maximum stresses significantly. For a given insulator shape, a higher value of electrode radius is found to reduce the maximum stresses in the presence of surface pollution for both configuration 1 and 2.

ACKNOWLEDGMENT

The authors wish to thank Alexander von Humboldt-Stiftung, Germany, as the work has been carried out at the Technical University Munich, Germany, where Dr. S. Chakravorti worked as Alexander von Humboldt-Stiftung research fellow.

REFERENCES

[1] P. K. Mukherjee and C. K. Roy, "Computation of fields in and around insulators by fictitious point charges", IEEE Trans. Electr. Insul., Vol. 13, pp. 24–31, 1978.

[2] M. J. Khan and P. H. Alexander, "Charge simulation modeling of practical insulator geometries", IEEE Trans. Electr. Insul., Vol. 17, pp. 325–332, 1982.

[3] S. Kaana - Nkusi, P. H. Alexander and R. Hackam, "Potential and electric field distribution at a HV insulator shed", IEEE Trans. Electr. Insul., Vol. 23, pp. 307–317, 1988.

[4] Z. Haznadar, S. Milojkovic and I. Kamenica, "Numerical field calculation of insulator chains for HV transmission lines", Paper no. 12.08, 3rd Int. Symp. on HV Engg., Milan, 1979.

[5] M. R. Iravani and M. R. Raghuveer, "Numerical computation of potential distribution along a transmission line insulator chain", IEEE Trans. Electr. Insul., Vol. 18, pp. 167–170, 1983.

[6] H. Singer, H. Steinbigler and P. Weiss, "A charge simulation method for the calculation of HV fields", IEEE Trans. on PAS, Vol. 93, pp. 1660–1668, 1974.

[7] M. Abdel-Salam and E. K. Stanek, "Optimising field stress on HV insulators", IEEE Trans. Electr. Insul., Vol. 22, pp. 47–56, 1987.

[8] H. Singer, "Impulse stresses of Conductive dielectrics", Paper no 11.02, 4th Int. Symp. on HV Engg., Athens, 1983.

[9] T. Takuma, T. Kawamoto and H. Fujinami, "Charge simulation method with complex fictitious charges for calculating capacitive-resistive fields", IEEE Trans. on PAS, Vol. 100, pp. 4665–4672, 1981.

[10] U. Kumar and G. R. Nagabhushana, "Solution of capacitive-resistive transient fields", Paper no. 8351, 9th Int. Symp. on HV Engg., Graz, 1995.

[11] S. Chakravorti and P. K. Mukherjee, "Power frequency and impulse field calculation around a HV insulator with uniform or non-uniform surface pollution", IEEE Trans. Electr. Insul., Vol. 28, pp. 43-53, 1993.

[12] L. Tang and M. R. Raghuveer, "E-field modeling of HVDC wall bushing performance", Paper no. 8324, 9th Int. Symp. on HV Engg., Graz, 1995.

[13] D. Beatovic, P. L. Levin, S. Sadovic and R. Hutnak, "A Galerkin formulation of the boundary element method for two-dimensional and axi-symmetric problems in electrostatics", IEEE Trans. Electr. Insul., Vol. 27, pp. 135-143, 1992.

[14] F. Gutfleisch, H. Singer, K. Förger and S. A. Gomollon, "Calculation of HV fields by means of the boundary element method", IEEE Trans. on PWRD, Vol. 9, pp. 743–749, 1994.

[15] Z. Andjelic, P. L. Levin, M. Spasojevic, H. Steinbigler and C. Trinitis, "Accelerated 3-D optimization of HV apparatus", Paper no. 8867, 9th Int. Symp. on HV Engg., Graz, 1995.

[16] S. Chakravorti and H. Steinbigler, "Capacitive-resistive field calculation around a HV insulator using boundary element method", Paper no. 3011, 10th Int. Symp. on HV Engg., Montreal, 1997.

[17] S. Chakravorti and H. Steinbigler, "Electric field calculation including surface and volume resistivities by boundary element method", Journal of the I. E. (India), Vol. 78, Pt. EI, pp. 17–23, 1997.

[18] S. Chakravorti and H. Steinbigler, "Capacitive-resistive field calculation in and around HV bushings by boundary element method", IEEE Trans. Dielectr. and EI, Vol. 5, pp. 237–244, 1998.

[19] K. Förger, *Integration verlustbehafteter Dielektrika in die Berechnung elektrischer Felder durch Integralgleichungsmethoden*, Doctoral Thesis, Technische Universität Hamburg-Harburg, Germany, 1998.

[20] F. Messerer and W. Boeck, "Field optimization of a HVDC-GIS spacer", Proc. IEEE CEIDP Conf., Atlanta, USA, Vol. 1, pp. 15–18, 1998.

[21] Z. Andjelic, B. Krstajic, S. Milojkovic, A Blaszczyk, H. Steinbigler and M. Wohlmuth, *Integral methods for the calculation of electric fields*, Scientific Series of the International Bureau, Vol. 10, Forschungszentrum Jülich GmbH, Germany, 1992.

[22] H. Singer, "Feldberechnung mit Oberflächenleitschichten und Volumenleitfähigkeit der Isolation", ETZ Archiv, BD 3, H8, pp. 265–267, 1981.

Manuscript was received on 28 May 1998, in final form 2 October 1999.